Characterisation of a Novel Light Activated Adhesive Scaffold: Potential for Device Attachment

Morris Ark, Giang T. Tran, Yong J. Chen, Philip Boughton, Peter H. Cosman, Colin R. Dunstan

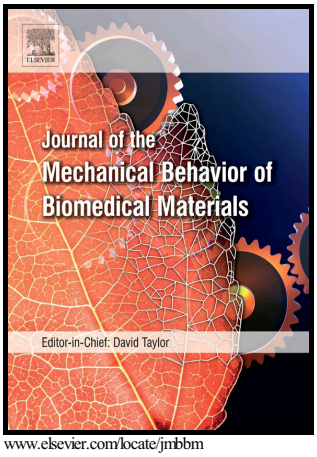

www.elsevier.com/locate/jmbbm

PII: S1751-6161(16)30157-6
DOI: http://dx.doi.org/10.1016/j.jmbbm.2016.05.029
Reference: JMBBM1942

To appear in: *Journal of the Mechanical Behavior of Biomedical Materials*

Received date: 28 February 2016
Revised date: 20 May 2016
Accepted date: 23 May 2016

Cite this article as: Morris Ark, Giang T. Tran, Yong J. Chen, Philip Boughton, Peter H. Cosman and Colin R. Dunstan, Characterisation of a Novel Ligh Activated Adhesive Scaffold: Potential for Device Attachment, *Journal of th Mechanical Behavior of Biomedical Materials* http://dx.doi.org/10.1016/j.jmbbm.2016.05.029

Characterisation of a Novel Light Activated Adhesive Scaffold: Potential for Device Attachment

Morris Ark[a], Giang T. Tran[b], Yong J. Chen[a], Philip Boughton[a], Peter H. Cosman[c,d], Colin R. Dunstan[a,*]

[a]Biomedical Engineering, School of Aerospace, Mechanical & Mechatronic Engineering, The University of Sydney, NSW 2006, Australia

[b] Faculty of Medicine, University of New South Wales, Ingham Institute of Applied Research, Liverpool NSW, 2170 Australia

[c] School of Medicine, University of Western Sydney, Campbelltown NSW 2560, Australia

[d]Liverpool Hospital NSW 2170, Australia

morris.ark@sydney.edu.au, g.tran@unsw.edu.au, yong.chen@sydney.edu.au, philip.boughton@sydney.edu.au, peter@cosman.org, colin.dunstan@sydney.edu.au*

*corresponding author

Keywords: scaffold; adhesion; tissue engineering; photoactive; sutures; wound healing

Abstract: The most common methods for attaching a device to the internal tissues of the human body are via sutures, clips or staples. These attachment techniques require penetration and manipulation of the tissue. Tears and leaks can often be a complication post-attachment, and scarring usually occurs around the attachment sites. To resolve these issues, it is proposed to develop a soft tissue scaffold impregnated with Rose Bengal/Chitosan solution (RBC-scaffold, 0.01% w/v Rose Bengal, 1.7% w/v Medium Molecular Weight Chitosan). This scaffold will initially attach to the tissue via a light activation method. The light activates the dye in the scaffold which causes cross-links to form between the scaffold and tissue, thus adhering them together. This is done without mechanically manipulating the surrounding tissue, thus avoiding the issues associated with current techniques. Eventually, the scaffold will be resorbed and tissue will integrate for long-term attachment.

A variety of tests were performed to characterise the RBC-scaffold. Porosity, interconnectivity, and mechanical strength were measured. Light activation was performed with a broad spectrum (380 – 780nm) 10W LED lamp exposed to various time lengths (2 – 15 mins, Fluence range 0.4 – 3 J/cm^2). Adhesive strength of the light-activated bond was measured with lap-shear tests performed on porcine stomach tissue. Cell culture viability was also assessed to confirm tissue integration potential. These properties were compared to Variotis™, an aliphatic polyester soft tissue scaffold which has proven to be viable for soft tissue regeneration.

The RBC-scaffolds were found to have high porosity (86.46 ± 2.95%) and connectivity, showing rapid fluid movement. The elastic modulus of the RBC-scaffolds (3.55 ± 1.28 MPa) was found to be significantly higher than the controls (0.15 ± 0.058 MPa, $p < 0.01$) and approached reported values for human gastrointestinal tissue (2.3 MPa). The maximum adhesion strength achieved of the RBC-scaffolds was 8.61 ± 2.81 kPa after 15 minutes of light activation, this is comparable to the adhesion strength of fibrin glue on scaffolds. Cell attachment was seen to be similar to the controls, but cells appeared to have better cell survivability.

RB – Rose Bengal

Corresponding Author: Colin Dunstan email: colin.dunstan@sydney.edu.au Tel: +61 2 9351 2127

In conclusion, the RBC-scaffolds show promise for use as a novel light activated attachment device with potential applications in attaching an anti-reflux valve in the lower oesophagus and also in wound healing applications for stomach ulcers.

1 Introduction:

Current methods for device attachment to soft tissue, often involve sutures, clips or staples (Quinn, 2005). These devices mechanically manipulate the surrounding tissue, placing unnecessary tension on the tissue site. This tension usually leads to leaks or tears post-surgery (Klink et al., 2011; Márquez et al., 2010). On top of these issues, the healed tissue will often result in scarring (Postlethwait et al., 1975). Biocompatible glues are an alternative adhesion method, but they often are degradable and not suitable for long-term fixation (Quinn, 2005). Along with the issues associated with device attachment, the implanted device itself can become encapsulated by fibrous tissue. This will usually occur if the device is not biocompatible, or is not fixed sufficiently (Sanders et al., 2000).

Soft tissue scaffolds have become a desirable method of repairing tissue using the patient's own cells (Chan and Leong, 2008). They are often biocompatible, bioresorbable, flexible and strong (O'Brien, 2011; Place et al., 2009). Porosity, interconnectivity and mechanical strength are important properties for the success of tissue engineering scaffolds (Khoda and Koc, 2012; O'Brien, 2011). A scaffold requires high porosity so that cells can penetrate the scaffold, as well as allow for vascularisation (Loh and Choong, 2013). Interconnectivity of the scaffold, the degree at which pores are connected to each other and the external environment, is an important property. It dictates whether cells can grow throughout the scaffold and whether sufficient nutrient and waste can be transported in and out of the scaffold (Phelps and Garcia, 2008). The mechanical properties of the scaffold must be strong enough to withstand the stresses that are expected *in vivo*, but not too strong that the properties outmatch the surrounding tissue, creating issues with cell differentiation and stress shielding. There is a trade-off that must be considered between porosity and strength (Chan and Leong, 2008; Hutmacher, 2000). Biocompatibility and the ability to be resorbed are important for the interaction with the human body and its long-term use. Variotis™, is a aliphatic polyester based soft tissue scaffold that has previously been used for wound repair studies (Ma et al., 2010; Zhang et al., 2013).

Rose Bengal (RB) dye is a biocompatible stain currently used most frequently for ophthalmology in diagnosing eye damage (Korb et al., 2008). Recently a novel use for RB dye has been described, taking advantage of its photoactive properties to adhere tissue after light activation (Chan et al., 2008). Tsao *et al*. has shown it to be successful in healing skin wounds with visibly less scarring compared to traditional sutures (Tsao et al., 2012). Lauto *et al.* has recently shown it to be effective in nerve repair (Lauto et al., 2008). Barton *et al.* has shown that rose bengal-chitosan film has negligible toxicity for cells (Barton et al., 2012). The shortcoming of its current use is that it has been used as film, which has low strength and high elastic modulus making it stiff and unsuitable for areas with a lot of movement in the body (Barton et al., 2014). Another issue with its current implementation is that green laser (532 nm) is used to activate the RB. This is because RB has absorbance peaks at 526 and 562 nm (Lauto et al., 2010). Using lasers has safety concerns with thermal damage to the surrounding tissue as well as potential eye damage to the operators (Sliney, 1995).

A novel soft tissue scaffold was created by combining Variotis™ and Rose Bengal, capable of adhering to tissue by simple light activation. The objective of this work was to characterise this novel tissue scaffold, and assess if it is appropriate for device attachment. The clinical application will be focussed on the gastro-intestinal tract, where there are a number of potential applications such as attachment of an anti-reflux valve in the lower oesophagus or patches to repair stomach perforations.

2 Materials/Method

2.1 Rose Bengal – Chitosan solution

The Rose Bengal - Chitosan solution (from here on referred to as RBC solution) was prepared following the method outlined by (Lauto et al., 2012). Briefly, 1.7% w/v of medium molecular weight chitosan was dissolved in deionised water containing 2% v/v acetic acid and 0.01% w/v Rose Bengal dye. The solution was stirred for 14 days at room temperature (25°C) to allow the Rose Bengal to dissolve, as it has poor solubility. The final RBC solution was then centrifuged at 3,270g for 1 hour at room temperature to remove any impurities. All processes involving the Rose Bengal were performed in the dark, or wrapped in aluminium foil to prevent photo-bleaching. Chan, *et al*. found that a concentration of 0.1% RB was superior for adhesive strength (Chan et al., 2002), therefore scaffolds made with 0.1% w/v RB were also prepared. All chemicals were sourced from Sigma-Aldrich, Sydney Australia.

2.2 RBC-Scaffold synthesis

Variotis™ scaffolds (Biometic Pty Ltd, Sydney, Australia) were prepared to the desired size of approximately 1.3mm thickness using a vibroslicer. The sliced scaffolds were then soaked in the previously prepared RBC solution overnight, and then subsequently dried over 2 weeks in a light shielded container. Control scaffolds were similarly prepared, but not soaked in RBC solution.

2.3 Scaffold characterisation

Scaffold morphology was examined with scanning electron microscopy (SEM) using a Zeiss Ultra+ (Carl Zeiss Microscopy GmbH, Germany) at 5 keV. The scaffolds were gold sputter coated and had silver painted on the edges to improve conductivity. Pore sizes were calculated from the SEM images using image processing software, ImageJ (National Institute of Health, MD, USA). Scaffold porosity was estimated using the following density calculations based on work by (Blaker et al., 2005):

$$\phi = 1 - \frac{\rho_{\text{scaffold}}}{\rho_{\text{polyester}}} = 1 - \frac{m_{\text{scaffold}}}{\rho_{\text{polyester}} V_{\text{scaffold}}} \qquad \text{(Eqn. 1)}$$

where ϕ = Porosity (%), ρ = density (g/cm^3), m = mass (g), and V = volume (cm^3).

The density of the polyester used was 1.145 g/cm^3 (Sigma-Aldrich).

Interconnectivity of the scaffolds was visualised using a capillarity test (Vitale-Brovarone et al., 2008). Briefly, it involved preparing a solution made up of 30% Fetal Bovine Serum (FBS), 70% distilled water and a few drops of blue food colouring to help visualisation. This solution is designed to have a similar viscosity to interstitial body fluid. The scaffolds were carefully placed into this solution. The flow of the solution into the scaffold was observed and recorded on video. After two minutes in the solution, the scaffold was removed and placed flat on absorbent paper. The leaching of the solution was observed and recorded on video. Afterwards the videos were analysed using Kinovea video analysis software (Kinovea, France) to record time in, time out and the general appearance of the scaffolds.

Further scaffold morphology analysis was performed using MicroCT with a Skyscan 1172 (Bruker microCT, Belgium), and the subsequent images were reconstructed and analysed using CTAn (Bruker microCT, Belgium). The scaffolds required Osmium Tetroxide vapour staining to improve the

contrast of the materials. The tensile properties of the scaffolds were measured using methods based on *ASTM D882 - Standard Test Method for Tensile Properties of Thin Plastic Sheeting* (International, 2012). Testing was conducted in an Instron 5567 Universal Testing machine (Instron, MA, USA) equipped with a 100 N load cell at a strain rate of 10 mm/min. Five samples were evaluated for each scaffold.

2.4 Scaffold Adhesion

To photo-activate the scaffolds and thus adhere them to tissue, a 10 W cool white broad spectrum LED lamp (Jaycar Electronics, Australia) was used. The white LED was selected as it is easily accessible, safe, and has a broad-spectrum wavelength incorporating the 532nm green wavelength required to activate the photoactive dye. The LED light source was characterised by using a Spectrascan® PR-730 spectroradiometer (Photoresearch Inc., USA) at 0.5° aperture and a S120VC Power Sensor (Thorlabs Inc., NJ, USA). The scaffolds were adhered to the mucosal side of porcine stomach tissue. Porcine stomach tissue was chosen for its relative accessibility and itsclose resemblance of human gastrointestinal tissue (Swindle et al., 2012). Attachment of devices in the stomach is one of the potential applications, another reason for the selection of porcine stomach tissue. To maximise adhesion and ensure tissue contact with the surface of the scaffold, a 1 kg mass was placed atop the scaffold during light exposure (Figure 1). As adhesion strength was expected to vary depending on exposure time, a series of times were tested (2, 5, 10, and 15 minutes). During light exposure tissue surface temperature was measured using a temperature probe. This was conducted to observe any potential thermal damage. Scaffold adhesion strength was evaluated using lap-shear tests based on *ASTM F2255 - Standard Test Method for Strength Properties of Tissue Adhesives in Lap-Shear by Tension Loading* (International, 2010). The adhesion strength was calculated using the equation for shear stress, $\tau = F/A$, where F was the highest force recorded before failure, and A was the adhesive surface area which was equal to the area of the scaffold. The scaffolds with 0.1% w/v RB were only tested at 2 and 10 minute light exposures for comparison.

2.5 Scaffold-Tissue interface visualisation

To observe the cross-links formed due to light activation, SEM images were taken of the interface between the scaffold and tissue. In preparation for SEM, samples were immediately fixed after light-activated adhesion in 2.5% glutaraldehyde for 1 hour, then 1% OsO_4 post-fixation for 1 hour. The samples were then dehydrated in a graded series of ethanol concentrations, HMDS (hexamethyldisilazane) dried, mounted on carbon and then sputter coated with gold. SEM was performed on a Zeiss Ultra at 5 keV.

2.6 Cell culture and proliferation

The ability of the scaffolds to support cell adhesion and growth was evaluated. Mouse skin fibroblast (3T3-L1) cells, were cultured in Dulbecco's Modified Eagle Medium (DMEM) supplemented with 1% penicillin, 1% streptomycin. Prior to seeding, the scaffolds were sterilised by immersion in 70% ethanol for 6 hours, followed by rinsing in Phosphate Buffered Saline (PBS) three times, and then pre-incubated in DMEM for 24 hours to improve cell attachment (Chatterjee et al., 2012). Scaffold samples were placed in 24-well culture plates and seeded with 1.5 x 10^5 cells/scaffold using the static surface seeding method (Thevenot et al., 2008). After seeding they were placed in incubation for 3 hours to allow for initial cell attachment and then immersed in supplemented DMEM for further cell growth (Thevenot et al., 2008). Culture medium was replaced every second day.

To assess cell attachment and survivability, SEM and Live/Dead Assay were performed. SEM was performed to observe cell morphology and attachment. The scaffolds were removed at 1, 3, and 7 days' culture, fixed in 2.5% glutaraldehyde for 24 hours at 4°C, dehydrated in a graded series of ethanol concentrations, dried with HMDS, and then sputter coated with gold. The electron microscope was operated at 5 keV to image the samples. Live/Dead Assay was performed by removing scaffold samples at each time interval, rinsing in PBS and then incubated in fluorescing solution (1ml PBS, 1µL calcein-AM and 1µL of Propidium Iodide) (Sigma-Aldrich) for 15 minutes. After incubation the scaffolds were placed under Olympus BX51 Fluorescence microscope (Olympus, Japan) and cells observed. Live cells appeared green, while dead cells appeared red. Live Cell images and Dead Cell images were overlayed on top of each other using ImageJ.

2.7 Statistical methods

Data are expressed as mean ± standard deviation. The two-sample *t*-test was used to interrogate the data for significance in differences.

3 Results & Discussion

3.1 Scaffold physical properties

The RBC-scaffold production process described above produced consistently sized and coated scaffolds which were bright pink in colour (Figure 3a). Table 1 summarises the various pore properties characterised. After coating, the mass of the scaffolds significantly increased ($p < 0.01$), this was expected as the coating adds to the mass. The volume did not change significantly ($p > 0.1$) which is a good sign that the dimensions of the scaffold do not change after the coating process. There was a significant decrease in porosity ($p < 0.01$) after the scaffolds are coated in RBC solution.

Examination under SEM (Figure 2) revealed that the RBC solution had created films between some of the pores in the scaffold, potentially accounting for the decreased porosity. Film forming on one side of the RBCscaffolds is desirable, as it allows consistent contact with the tissue, thus improving adhesion. The SEM images also revealed many pores remain not blocked in the RBC-scaffold, so there is still a degree of interconnectivity. The other side of the scaffold has no film covering, so still allows for tissue integration and attachment to occur on that side. The average pore size and range were significantly smaller in the Variotis control, compared to the RBC-scaffold ($p < 0.01$). The SEM images revealed that the smaller pores in the RBC-scaffold are often covered over by the RBC film, and therefore explain why there is a shift to the larger pore sizes. The shift in pore size could affect the scaffolds cell attachment as certain cells prefer smaller pores, and larger pores decreases the surface area for the cells to attach to (Murphy and O'Brien, 2010). There is a limitation in using the SEM images for pore size analysis, since they only reveal surface pores and are only 2D measurements but they still provide a good indication of the general porosity of the scaffolds.

Table 1 - Scaffold Pore dimensions determined by SEM and density measurements

Scaffold Type	Mass (mg)	Volume (cm^3)	Porosity (%)	Pore Size Range (µm) [mean size]
Sliced Variotis	36 ± 4.90	0.562 ± 0.14	94.2 ± 0.94	120.7 - 684 [345]
RBC-scaffold	96 ± 1.20	0.649 ± 0.14	86.5 ± 2.95	213 - 967 [444]

Table 2 – Results of the Capillarity test determining the saturation (time in) and leaching (time out) times for Variotis and RBC-scaffolds

Scaffold Type	Time In (s)	Time Out (s)	Notes
Sliced Variotis	2.29 ± 0.809	10.59 ± 4.12	No noticeable trapped solution.
RBC-scaffold	0.545 ± 0.185	13.42 ± 3.90	Darkly stained blue, no trapped solution

Table 2 summarises the observations made during the capillarity test. Comparing the sliced Variotis to the RBC-scaffold, the time it takes for the blue solution to saturate the RBC-scaffold is significantly shorter ($p < 0.05$), but the time for the solution to leach out shows no significant difference ($p > 0.1$). This means the interconnectivity of the two scaffold types are comparable and sufficient for waste transport. Interestingly the RBC-scaffolds were significantly stained blue after the test (Figure 3c), whereas the controls did not stain significantly (Figure 3b). The quicker uptake of solution and staining could be attributed to the hydrophilic chitosan in the RBC coating absorbing the solution (García Cruz et al., 2008).

Effective interconnectivity is necessary for the transport of nutrients and waste in tissue engineering. The drop in porosity to ~85% for the RBC-scaffold is not a major concern as it has been shown that porosity >70% is sufficient to allow nutrient transport and tissue ingrowth (Yang et al., 2001).

MicroCT analysis further reinforced the results found from the physical measurements and SEM. The porosity in the control scaffold is high with great interconnectivity throughout the scaffold. The RBC-scaffold, showed signs of coated struts with some pores being blocked by film (Figure 4), it also revealed that the RBC-scaffold still had 100% interconnectivity.

3.2 Scaffold mechanical properties

The mechanical properties of the scaffolds are summarised in Table 3. The RBC-scaffold was found to be significantly stiffer than any of the other samples ($p < 0.01$), even greater than the literature values for human oesophagus (Vanags et al., 2003). Yield strength was also significantly increased from the control ($p < 0.05$), but did not reach the strength of the porcine stomach tissue tested. The increase in stiffness and strength can be attributed to the RBC-coating, forming film and joining struts together within the scaffold.

Scaffold design often requires a compromise between mechanical properties and porosity. A scaffold which is too porous will often not have enough mechanical strength; while a scaffold which has high modulus will often have little porosity to support tissue growth. The RBC-scaffold has a compromise of lower porosity but stronger mechanical properties, which match the properties of gastrointestinal tissue closely giving it a better chance for tissue integration.

Figure 5, shows sample stress-strain curves of both the sliced Variotis and RBC-scaffolds. The general shapes of the stress-strain curve for the two scaffold types are quite different. The Variotis scaffolds quickly decline in strength after yielding, while the RBC-scaffolds plateau after yielding, then decline. This plateau region represents the coated struts of the RBC-scaffold delaying sudden fracture. By contrast, the Variotis control has no coating, resulting in each strut of the scaffold fracturing quickly. This gives the RBC-scaffolds more tolerance to immediate failure, as the coating helps maintain the strength of the scaffold. This makes the RBC-scaffold more suitable for device attachment. Compared to the conventional film design by Lauto et al., the scaffold structure has lower

stiffness (3.55 ± 1.28 vs. 16.0 ± 4.7 kPa (Barton et al., 2014)). The flexibility is attributed to the struts of the scaffold able to deform slightly before failure. This lower stiffness makes it more compatible for tissue integration.

Table 3 - Mechanical properties of the scaffolds found after tensile test, compared against literature values.

Summary	Elastic Modulus (MPa)	Yield (kPa)
Sliced Variotis	0.1509 ± 0.058	11.93 ± 6.15
RBC-scaffold	3.55 ± 1.28	94.58 ± 39.48
Porcine Stomach	1.073 ± 0.40	226.8 ± 54.20
Literature. Human oesophagus (Vanags et al., 2003)	2.3	2190
RBC Film design (Barton et al., 2014)	16.0 ± 4.7	8100 ± 1900

3.3 Scaffold adhesion strength

The exact mechanism for protein–protein cross-linking initiated by light absorption of RB molecules has not been fully elucidated. The general theory is that light is absorbed by the RB, which promotes it to an excited singlet, then excited triplet state. When sufficient oxygen is present, the RB triplet state transfers energy to oxygen, generating singlet oxygen. This singlet oxygen then reacts with certain amino acids, mainly histidine (His), to initiate covalent bonds between protein molecules (Cherfan et al., 2013; Shen et al., 2000). Since the bonds are made between protein molecules, the addition of chitosan in the RBC scaffold is essential. Scaffolds soaked in only RB do not achieve adhesion after light activation; this is because the tissue has no corresponding molecules for cross-linking.

The spectral power distribution measured by the spectroradiometer is shown in Figure 6. The curve is typical of a blue-phosphor LED, with peaks in the blue and green-yellow region. The power meter measured 3.43mW/cm^2 of irradiance at the 532nm wavelength (the peak wavelength absorbed by RB). Taking into consideration the exposure times of 2 - 15 min, the fluence range was 0.4 - 3 J/cm^2. This is considerably lower than the energy used by laser activation which is usually ~100 J/cm^2 (Lauto et al., 2010; Xu et al., 2015). Adhesion was successful after light activation with the broad spectrum LED. This shows that it is not necessary to use high powered lasers to photoactivate the dye. This is beneficial to the methods usability as it minimises thermal damage and avoids eye safety concerns. It is also a cheaper and more accessible option compared to lasers. Martinez *et al.* also showed great success in using non-laser activation for photochemical tissue bonding. They found that the bonding strength formed via a 50W halogen lamp and corresponding coloured filters was equivalent to the strength formed via laser activation (Martínez-Escanamé et al., 2008).

The results of the lap shear adhesion test indicate that the adhesive bond strength increases as the light exposure time increases. The results of the adhesion test are summarised in Table 4. The increase in strength between each time interval was found to be not statistically significant ($p > 0.1$) except for the increase from 5 min to 10 min ($p < 0.05$). The maximum adhesion strength achieved with the RBC-scaffold (8.61 ± 2.81 after 15min LED activation) isn't far off from the adhesion achieved by RBC film tested by (Lauto et al., 2010) who achieved adhesion strength of 15.1 ± 1.2 kPa after 6 minutes of laser activation.

Yang, *et al.* using FEM (Finite Element Modelling), simulated a 5ml bolus being transported through an oesophagus under peristalsis and found that the highest axial and circumferential stress are 29.0 and 36.5 kPa respectively. They also found that the highest shear stress was 238.6 Pa (Yang et al., 2007). Based on the adhesive shear strength results for the RBC-scaffold, it is expected that the scaffolds will withstand these *in vivo* shear stresses. It should however be noted that *in-vivo* forces will be multi-directional, while this test only applied forces in one direction.

Knecht *et al.* compared the strength of various scaffold fixation techniques (press-fit, cartilage sutures, fibrin glue and transosseous sutures) and found that transosseous sutures were the strongest, withstanding 38.18 ± 9.53 N of tensile force. Fibrin glue was found to withstand 2.18 ± 0.47 N of tensile load and chondral sutured scaffolds were 26.29 ± 1.55 N (Knecht et al., 2007). The light-activated adhesive method is comparably in strength to fibrin glue (converting the fibrin glue force to shear stress is ~13kPa), but still cannot beat the current standard of sutures. The RBC-scaffold isn't expected to be placed in areas of high mobility, so it isn't required to be as strong as sutures.

The difference between the two concentrations was unexpected. Based on the work by Chan *et al.*, it was assumed that a higher concentration of RB would allow for more cross-links to form. This however was not the case, with the 10 min 0.1% w/v samples matching up to the 5 min 0.01% w/v samples in adhesion strength. This difference could be attributed to the additional concentration of RB, oversaturating the scaffold and actually interfering with the interactions that occur between the molecules on the tissue and scaffold. This was also noted by Chan et al. when they were discussing why higher concentrations of RB did not result in stronger bonds (Chan et al., 2002). The oversaturation can be seen by the appearance of the 0.1% RB tissue samples after lap shear testing (Figure 7b).

Table 4 - Adhesive Shear Strength for RBC-scaffold at various light exposure conditions after lap-shear tests

Scaffold	Exposure Time	Adhesive Shear Strength (kPa)	Notes
RB 0.01%	2 min	1.50 ± 1.21	2 samples failed during test prep.
	5 min	3.24 ± 3.28	2 samples failed during test prep.
	10 min	7.50 ± 0.99	1 sample failed cohesively
	15 min	8.61 ± 2.81	2 samples failed cohesively
RB 0.1%	2 min	1.93 ± 2.00	3 samples failed during test prep.
	10 min	3.01 ± 1.23	1 sample failed during test prep.

There were several issues with the adhesion test. Firstly, excessive variability in adhesion strength between samples was observed, this is especially evident in the shorter exposed samples. Secondly, inadvertent stress placed on the bonds during mounting of the specimens resulted in failure of some of the weaker samples prior to commencement of the tests; these results are noted. The strength of the bond for these samples was given at least 0.5 kPa. This represents the adhesive strength required to support the mass of the test fixture, and since all samples were able to support the fixture, this was chosen as the minimum bond strength.

For some samples of the longer exposure times, the failure of the bond actually occurred cohesively (i.e. the scaffold failed, not the adhesive bond). Figure 7a shows the scaffold still attached to the tissue but due to the failure of the scaffold it is missing a portion in the centre. This means the bond was limited by the strength of the scaffold at those times. This is also noted in the results.

3.4 Temperature change due to light actvation

Figure 8 shows the average temperatures reached for the various times tested. It can be seen that after 15 mins of exposure the temperature increased by 12.1°C. This increase in temperature is attributed to the use of a broad spectrum light source. RB absorbs light in the green region (532nm), that means the other wavelengths of light are not absorbed and that energy is converted to heat. Temperatures above 40°C can be damaging to tissue, with every 1°C rise doubling the rate of cellular death (Dewhirst et al., 2003; Li et al., 1987). This means the light activation system in its current form could cause thermal damage after prolonged activation. The temperature increases *in vivo* however, are expected to be different due to the difference in starting temperature (25°C vs 37°C) and the body's fluid cooling against temperature change. For initial *in vitro* tests and proof of concept the use of the broad spectrum LED lamp is acceptable, but for *in vivo* tests the light activation system will need to be modified to avoid thermal damage. This could involve using infrared filters, narrow wavelength sources or lower powered light sources. *In vivo* the scaffolds will need to be activated via endoscope, so the effect that has on adhesion will need to be assessed in future tests. Martinez et al. used a broad-spectrum 50W halogen lamp with coloured filters to activate RB dye. They found that after 10 minutes of activation at 0.1 W/cm^2 the surface temperature of the tissue increased from 27°C to 47°C, which they considered safe as it was below 60°C, the critical temperature for cell death for short periods of heating (Martínez-Escanamé et al., 2008).

3.5 Scaffold-Tissue interface

Representative SEM images of the scaffold-tissue interface are presented in Figures 9 & 10. Unless stated otherwise the images are orientated so that the top half is the RBC-scaffold, and the bottom half is the porcine stomach tissue. The micrographs further reinforce the results of the adhesive strength tests (Section 3.3). As exposure time increases, the interface between the tissue and scaffold becomes less pronounced, as more bonds are formed and the gap narrows. This can especially be seen when comparing the 2 min sample and 10 min samples for 0.01% RB (Figure 9a & Figure 9c). In the 2 min sample the bonds can be seen, whereas in the 10 min sample the interface gap is unnoticeable.

Comparing the two different concentrations of RB, the 2 min samples are comparable, with fewer bonds observed between the scaffold and tissue. The 10 min samples however, have stark differences. The 0.01% RB samples (Figure 9c) were more closely bonded to the tissue, while the 0.1% RB samples (Figure 10b) still have a distinct gap between scaffold and tissue. The 10 min 0.1% RB sample is more comparable to the 5 min 0.01% RB sample (Figure 9b), and this reinforces the adhesive strength results where the strength of the 0.1% RB samples were similar in strength to the 5 min 0.01% RB samples.

3.6 Scaffold cell culture tests

From the SEM images of cell attachment (Figure 11), it can be seen that both scaffolds support cell adhesion, as the morphology of the cells changed from spherical to flat spreading cells over the 7 days. All images are at 500x magnification. With regards to cell proliferation, the 0.01% w/v RBC scaffold appears to have poorer cell proliferation compared to the control when observing the number of cells with SEM.

Observing the Live/Dead Assay results (Figure 12), it can be seen that the control has significantly more dead cells over the 7 days compared to the RBC-scaffold. This indicates that the RBC coating is

more biocompatible and less cytotoxic than the control. This is a favourable sign for cell survival and tissue integration. The increase in biocompatibility can be attributed to the chitosan in the RBC coating being more hydrophilic, which improves cell spreading and survival (Chang and Wang, 2011). Previous studies have shown that chitosan treatment enhances cell attachment and proliferation, due to its increase in biocompatibility (Jing et al., 2014; Mei et al., 2005). Overall cell attachment and proliferation appear to be poorer in the RBC-scaffold, this was also observed in the SEM images. This could be due to the larger pore sizes reducing surface area to volume ratio. A low surface area/volume ratio has been recognised for poor cell attachment as it minimises the surfaces for the cells to attach to (Bertoldi et al., 2011; Kim and Mooney, 1998). A possible way to improve the cell attachment is through addition of bioactive components such as bioglass or growth factors. In general, the cell interactions with the RBC-scaffold show great signs for the long-term tissue integration of the scaffold, allowing for a strong fixation.

4 Conclusion

In summary, the synthesis of a light-activated adhesive scaffold has been demonstrated. The scaffold's porosity and mechanical strength are sufficient for tissue integration. After light activation the RBC-scaffolds were able to adhere to porcine stomach tissue with adhesive strength sufficient to resist forces expected *in vivo*. LED light exposure was shown to be capable of activating the cross-linking process, but the heat produced by the lamp will need to be mitigated for *in vivo* trials. Cell culture tests revealed that the RBC coating enhanced biocompatibility. These promising results support using the RBC scaffold as a device attachment system, particularly in the gastro-intestinal tract. Further investigations using simulated models and *in vivo* animal studies are required before the device can be proven for clinical use. Due to its tissue engineering function, its applications could be outreaching, potentially useful as a wound healing patch to treat perforations.

5 Acknowledgements

The authors acknowledge the facilities and the scientific and technical assistance of the Australian Microscopy & Microanalysis Research Facility at the Australian Centre for Microscopy & Microanalysis,Wenye Hu from the Lightning Lab at the Faculty of Architecture, Design and Planning, and Kevin Cooke from the Interdisciplinary Photonics Lab, all located at the University of Sydney. This research was self-funded.

6 Conflict of Interest

There are no conflicts of interest to report.

7 References

Barton, M., Piller, S.C., Mahns, D.A., Morley, J.W., Mawad, D., Longo, L., Lauto, A., 2012. In vitro cell compatibility study of rose bengal–chitosan adhesives. Lasers in Surgery and Medicine 44, 762-768. doi: 10.1002/lsm.22076

Barton, M.J., Morley, J.W., Mahns, D.A., Mawad, D., Wuhrer, R., Fania, D., Frost, S.J., Loebbe, C., Lauto, A., 2014. Tissue repair strength using chitosan adhesives with different physical-chemical characteristics. Journal of Biophotonics 7, 948-955. doi: 10.1002/jbio.201300148

Bertoldi, S., Farè, S., Tanzi, M.C., 2011. Assessment of scaffold porosity: the new route of micro-CT. Journal of Applied Biomaterials & Biomechanics 9, 165-175. doi: 10.5301/JABB.2011.8863

Blaker, J.J., Maquet, V., Jérôme, R., Boccaccini, A.R., Nazhat, S.N., 2005. Mechanical properties of highly porous PDLLA/Bioglass® composite foams as scaffolds for bone tissue engineering. Acta Biomaterialia 1, 643-652. doi: http://dx.doi.org/10.1016/j.actbio.2005.07.003

Chan, B.P., Chan, O.C.M., So, K.F., 2008. Effects of photochemical crosslinking on the microstructure of collagen and a feasibility study on controlled protein release. Acta Biomaterialia 4, 1627-1636. doi: http://dx.doi.org/10.1016/j.actbio.2008.06.007

Chan, B.P., Kochevar, I.E., Redmond, R.W., 2002. Enhancement of Porcine Skin Graft Adherence Using a Light-Activated Process. Journal of Surgical Research 108, 77-84. doi: http://dx.doi.org/10.1006/jsre.2002.6516

Chan, B.P., Leong, K.W., 2008. Scaffolding in tissue engineering: general approaches and tissue-specific considerations. European Spine Journal 17, 467-479. doi: 10.1007/s00586-008-0745-3

Chang, H.-I., Wang, Y., 2011. Cell responses to surface and architecture of tissue engineering scaffolds. INTECH Open Access Publisher.

Chatterjee, K., Hung, S., Kumar, G., Simon, C.G., 2012. Time-Dependent Effects of Pre-Aging 3D Polymer Scaffolds in Cell Culture Medium on Cell Proliferation. Journal of Functional Biomaterials 3, 372-381. doi: 10.3390/jfb3020372

Cherfan, D., Verter, E.E., Melki, S., Gisel, T.E., Doyle, J.F.J., Scarcelli, G., Yun, S.H., Redmond, R.W., Kochevar, I.E., 2013. Collagen Cross-Linking Using Rose Bengal and Green Light to Increase Corneal StiffnessCollagen Cross-Linking to Augment Corneal Stiffness. Investigative Ophthalmology & Visual Science 54, 3426-3433. doi: 10.1167/iovs.12-11509

Dewhirst, M., Viglianti, B., Lora-Michiels, M., Hanson, M., Hoopes, P., 2003. Basic principles of thermal dosimetry and thermal thresholds for tissue damage from hyperthermia. International Journal of Hyperthermia 19, 267-294. doi: 10.1080/026567031000119006

García Cruz, D.M., Coutinho, D.F., Costa Martinez, E., Mano, J.F., Gómez Ribelles, J.L., Salmerón Sánchez, M., 2008. Blending polysaccharides with biodegradable polymers. II. Structure and biological response of chitosan/polycaprolactone blends. Journal of Biomedical Materials Research Part B: Applied Biomaterials 87B, 544-554. doi: 10.1002/jbm.b.31142

Hutmacher, D.W., 2000. Scaffolds in tissue engineering bone and cartilage. Biomaterials 21, 2529-2543. doi: http://dx.doi.org/10.1016/S0142-9612(00)00121-6

International, A., 2010. ASTM F2255-05(2010), Standard Test Method for Strength Properties of Tissue Adhesives in Lap-Shear by Tension Loading. ASTM International, West Conshohocken, PA. doi: 10.1520/F2255-05R10

International, A., 2012. ASTM D882-12, Standard Test Method for Tensile Properties of Thin Plastic Sheeting, West Conshohocken, PA,. doi: 10.1520/D0882-12

Jing, X., Mi, H.-Y., Cordie, T., Salick, M., Peng, X.-F., Turng, L.-S., 2014. Fabrication of Porous Poly(ε-caprolactone) Scaffolds Containing Chitosan Nanofibers by Combining Extrusion Foaming, Leaching, and Freeze-Drying Methods. Industrial & Engineering Chemistry Research 53, 17909-17918. doi: 10.1021/ie5034073

Khoda, A.K.M.B., Koc, B., 2012. Designing Controllable Porosity for Multifunctional Deformable Tissue Scaffolds. Journal of Medical Devices 6, 031003-031003. doi: 10.1115/1.4007009

Kim, B.-S., Mooney, D.J., 1998. Development of biocompatible synthetic extracellular matrices for tissue engineering. Trends in Biotechnology 16, 224-230. doi: http://dx.doi.org/10.1016/S0167-7799(98)01191-3

Klink, C., Binnebosel, M., Alizai, H., Lambertz, A., vonTrotha, K., Junker, E., Disselhorst-Klug, C., Neumann, U., Klinge, U., 2011. Tension of knotted surgical sutures shows tissue specific rapid loss in a rodent model. BMC Surgery 11, 36. doi: Artn 36 10.1186/1471-2482-11-36

Knecht, S., Erggelet, C., Endres, M., Sittinger, M., Kaps, C., Stüssi, E., 2007. Mechanical testing of fixation techniques for scaffold-based tissue-engineered grafts. Journal of Biomedical Materials Research Part B: Applied Biomaterials 83B, 50-57. doi: 10.1002/jbm.b.30765

Korb, D.R., Herman, J.P., Finnemore, V.M., Exford, J.M., Blackie, C.A., 2008. An Evaluation of the Efficacy of Fluorescein, Rose Bengal, Lissamine Green, and a New Dye Mixture for Ocular Surface Staining. Eye & Contact Lens 34, 61-64. doi: 10.1097/ICL.0b013e31811ead93

Lauto, A., Foster, L.J., Avolio, A., Sampson, D., Raston, C., Sarris, M., McKenzie, G., Stoodley, M., 2008. Sutureless nerve repair with laser-activated chitosan adhesive: a pilot in vivo study. Photomedicine and laser surgery 26, 227-234. doi: 10.1089/pho.2007.2131

Lauto, A., Mawad, D., Barton, M., Gupta, A., Piller, S.C., Hook, J., 2010. Photochemical tissue bonding with chitosan adhesive films. Biomedical engineering online 9, 47-47. doi: 10.1186/1475-925X-9-47

Lauto, A., Stoodley, M., Barton, M., Morley, J.W., Mahns, D.A., Longo, L., Mawad, D., 2012. Fabrication and Application of Rose Bengal-chitosan Films in Laser Tissue Repair. JoVE, p. e4158. doi: doi:10.3791/4158

Li, D.-J., Zhou, S.-L., Qiu, S.-L., Qiao, S.-J., 1987. Thermodamage, thermosensitivity and thermotolerance of normal swine oesophagus. International journal of hyperthermia 3, 143-151.

Loh, Q.L., Choong, C., 2013. Three-Dimensional Scaffolds for Tissue Engineering Applications: Role of Porosity and Pore Size. TISSUE ENGINEERING PART B-REVIEWS 19, 485-502. doi: 10.1089/ten.teb.2012.0437

Ma, Y., Bryce, N.S., Whan, R.M., Xiao, L., Li, K., Ruys, A.J., Hambley, T.W., Boughton, P., 2010. Growth of DLD-1 colon cancer cells on Variotis™ scaffolds of controlled porosity: A preliminary study. Journal of Biomimetics, Biomaterials, and Tissue Engineering 8, 79-89. doi: 10.4028/www.scientific.net/JBBTE.8.79

Márquez, M., Ayza, M., Lozano, R., del Mar Rico Morales, M., García Díez, J., Poujoulet, R., 2010. Gastric Leak After Laparoscopic Sleeve Gastrectomy. OBES SURG 20, 1306-1311. doi: 10.1007/s11695-010-0219-7

Martínez-Escanamé, M., Martínez-Ramírez, J., Aguilar-Hernández, G., Fuentes-Ahumada, C., Torres-Alvarez, B., Moncada, B., Castanedo-Cázares, J.P., González, F., 2008. Non-laser approach to photochemical tissue bonding. Revista mexicana de física 54, 173-175.

Mei, N., Chen, G., Zhou, P., Chen, X., Shao, Z.-Z., Pan, L.-F., Wu, C.-G., 2005. Biocompatibility of Poly(ε-caprolactone) Scaffold Modified by Chitosan—The Fibroblasts Proliferation in vitro. Journal of Biomaterials Applications 19, 323-339. doi: 10.1177/0885328205048630

Murphy, C.M., O'Brien, F.J., 2010. Understanding the effect of mean pore size on cell activity in collagen-glycosaminoglycan scaffolds. Cell Adhesion & Migration 4, 377-381. doi: 10.4161/cam.4.3.11747

O'Brien, F.J., 2011. Biomaterials & scaffolds for tissue engineering. Materials Today 14, 88-95. doi: http://dx.doi.org/10.1016/S1369-7021(11)70058-X

Phelps, E.A., Garcia, A.J., 2008. Update on therapeutic vascularization strategies. Regenerative Medicine 4, 65-80. doi: 10.2217/17460751.4.1.65

Place, E.S., George, J.H., Williams, C.K., Stevens, M.M., 2009. Synthetic polymer scaffolds for tissue engineering. Chemical Society Reviews 38, 1139-1151. doi: 10.1039/B811392K

Postlethwait, R.W., Willigan, D.A., Ulin, A.W., 1975. Human tissue reaction to sutures. Annals of Surgery 181, 144-150.

Quinn, J.V., 2005. Tissue Adhesives in Clinical Medicine. BC Decker, Incorporated.

Sanders, J.E., Stiles, C.E., Hayes, C.L., 2000. Tissue response to single-polymer fibers of varying diameters: Evaluation of fibrous encapsulation and macrophage density. Journal of Biomedical Materials Research 52, 231-237. doi: 10.1002/1097-4636(200010)52:1<231::AID-JBM29>3.0.CO;2-E

Shen, H.-R., Spikes, J.D., Smith, C.J., Kopeček, J., 2000. Photodynamic cross-linking of proteins: IV. Nature of the His–His bond(s) formed in the rose bengal-photosensitized cross-linking of N-benzoyl-L-histidine. Journal of Photochemistry and Photobiology A: Chemistry 130, 1-6. doi: http://dx.doi.org/10.1016/S1010-6030(99)00200-2

Sigma-Aldrich, 2013. Polycaprolactone, MSDS No. 440744. Sigma-Aldrich.

Sliney, D.H., 1995. Laser safety. Lasers in Surgery and Medicine 16, 215-225. doi: 10.1002/lsm.1900160303

Swindle, M.M., Makin, A., Herron, A.J., Clubb, F.J., Frazier, K.S., 2012. Swine as Models in Biomedical Research and Toxicology Testing. Veterinary Pathology Online 49, 344-356. doi: 10.1177/0300985811402846

Thevenot, P., Nair, A., Dey, J., Yang, J., Tang, L., 2008. Method to Analyze Three-Dimensional Cell Distribution and Infiltration in Degradable Scaffolds. Tissue Engineering. Part C, Methods 14, 319-331. doi: 10.1089/ten.tec.2008.0221

Tsao, S., Yao, M., Tsao, H., Henry, F.P., Zhao, Y., Kochevar, J.J., Redmond, R.W., Kochevar, I.E., 2012. Light-activated tissue bonding for excisional wound closure: a split-lesion clinical trial. British Journal of Dermatology 166, 555-563. doi: 10.1111/j.1365-2133.2011.10710.x

Vanags, I., Petersons, A., Ose, V., Ozolanta, I., Kasyanov, V., Laizans, J., Vjaters, E., Gardovskis, J., Vanags, A., 2003. Biomechanical properties of oesophagus wall under loading. Journal of biomechanics 36, 1387-1390.

Vitale-Brovarone, C., Miola, M., Balagna, C., Verné, E., 2008. 3D-glass–ceramic scaffolds with antibacterial properties for bone grafting. Chemical Engineering Journal 137, 129-136. doi: http://dx.doi.org/10.1016/j.cej.2007.07.083

Xu, N., Yao, M., Farinelli, W., Hajjarian, Z., Wang, Y., Redmond, R.W., Kochevar, I.E., 2015. Light-activated sealing of skin wounds. Lasers Surg Med 47, 17-29. doi: 10.1002/lsm.22308

Yang, S., Leong, K.-F., Du, Z., Chua, C.-K., 2001. The design of scaffolds for use in tissue engineering. Part I. Traditional factors. Tissue engineering 7, 679-689. doi: http://dx.doi.org/10.1089/107632701753337645

Yang, W., Fung, T.C., Chian, K.S., Chong, C.K., 2007. Finite element simulation of food transport through the esophageal body. World Journal of Gastroenterology 13, 1352-1359.

Zhang, M., Boughton, P., Rose, B., Lee, C.S., Hong, A.M., 2013. The use of porous scaffold as a tumor model. International journal of biomaterials 2013. doi: http://dx.doi.org/10.1155/2013/396056

8 Figure Legends

Figure 1 - Diagram of light activation using broad spectrum LED light. Weights were placed to maintain intimate contact between the tissue surface and the RBC-scaffold.

Figure 2 - SEM images of a) Control Variotis b) RBC-scaffold with pore blockage circled. Magnification 50x

Figure 3 – Appearance of a) 0.01% w/v RBC-scaffold before capillarity test b) Control scaffold after capillarity test c) RBC-scaffold after capillarity test.

Figure 4 – Sectioned view of a MicroCT reconstruction of 0.01% w/v RBC-scaffold. Pseudo-colour added based on the different thresholds distinguishing between the RBC coating and the base scaffold. Blue is scaffold, yellow is RBC coating.

Figure 5 – Sample Stress-Strain curve for Variotis and RBC-scaffolds after tensile test at a strain rate of 10mm/min.

Figure 6 – Normalised Spectral Power Distribution of the Cool White LED lamp used for light activation

Figure 7 – a) RB 0.01% scaffold exposed to 15 min of light, failed cohesively b) Comparison of the stain after adhesion test, left is RB 0.01%, right is RB 0.1%.

Figure 8 - Tissue Surface Temperatures reached after certain times of LED exposure

Figure 9 - SEM of 0.01% RBC-scaffold interface after a) 2 min, arrows highlighting the cross-links formed b) 5 min, c) 10 min arrows highlighting intimate interface and d) 15 min light exposure. Top half is RBC scaffold, bottom is porcine stomach tissue.

Figure 10 - SEM of 0.1% RBC-scaffold interface after a) 2 min and b) 10 min light exposure. The interface between the scaffold (top) and tissue (bottom) is less intimate compared to the 0.01% samples

Figure 11 - SEM images observing cell morphology over 7 days on the surface of a) Variotis scaffolds b) RBC-scaffold. Cells seeded were mouse skin fibroblasts (3T3-L1). Magnification 500x

Figure 12 - Live/Dead Assay of mouse skin fibroblasts (3T3-L1) on a) Variotis scaffolds b) RBC scaffolds. Calcein was used for the green fluorescence of live cells, and Propidium Iodide was used for the red fluorescence of dead cells. Magnification 40x.

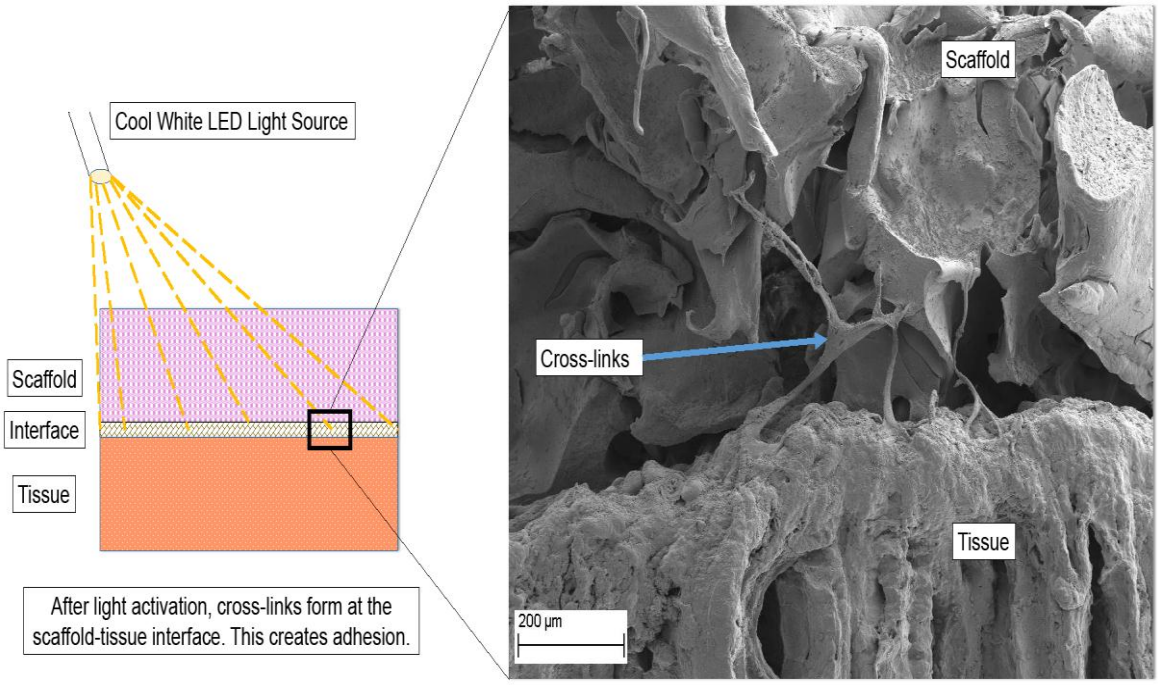

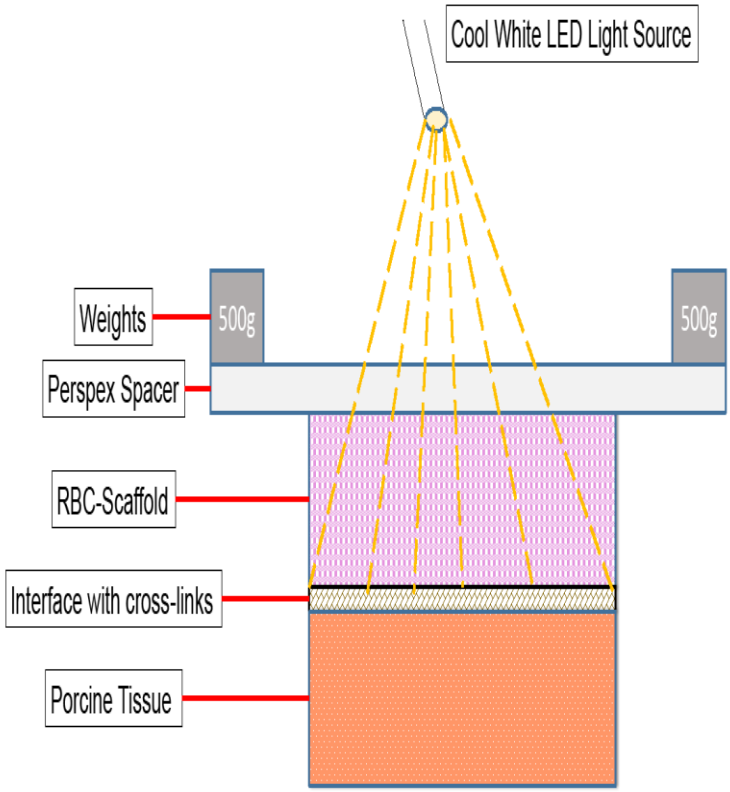
Cool White LED Light Source
Weights
500g
500g
Perspex Spacer
RBC-Scaffold
Interface with cross-links
Porcine Tissue

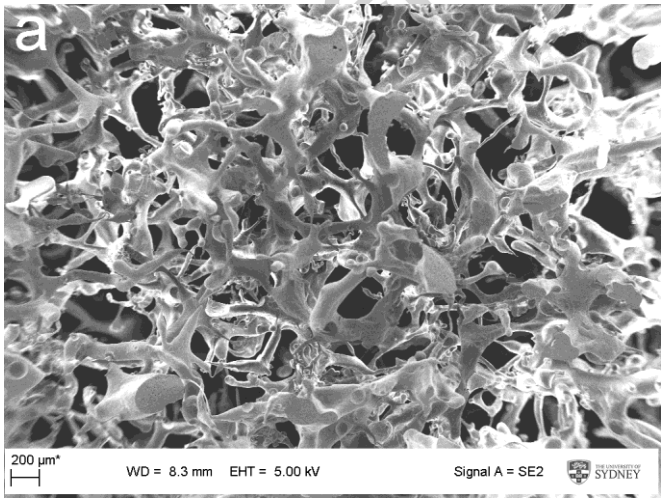
a
200 µm*
WD = 8.3 mm
EHT = 5.00 kV
Signal A = SE2
THE UNIVERSITY OF SYDNEY

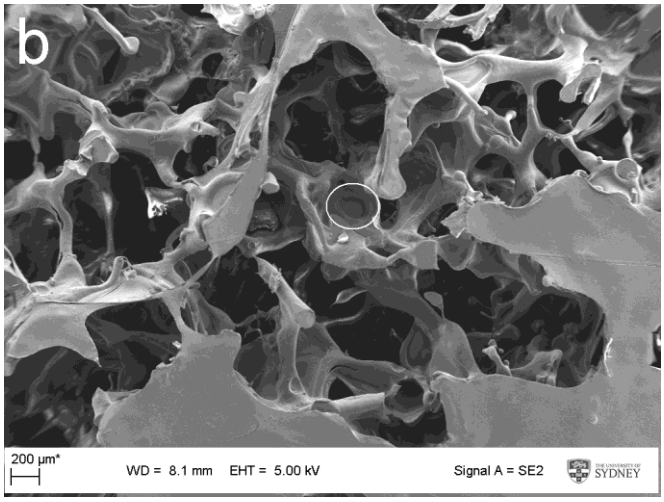

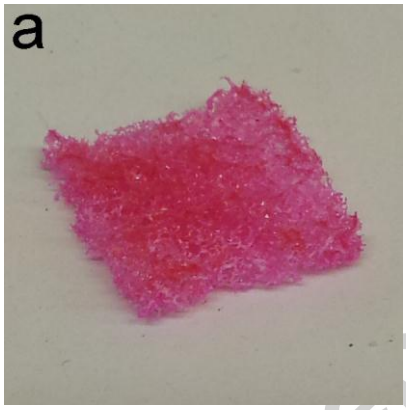

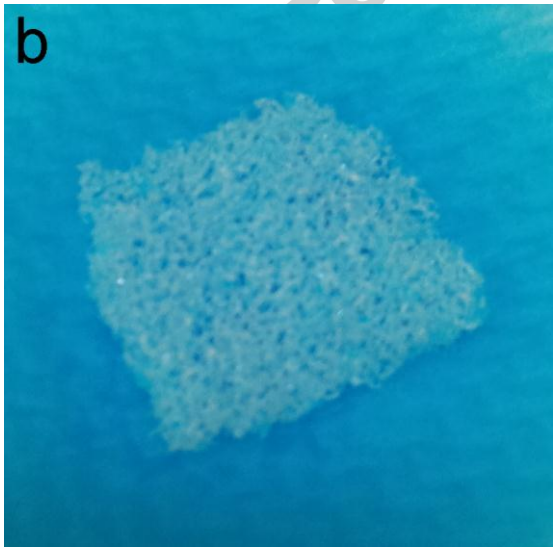

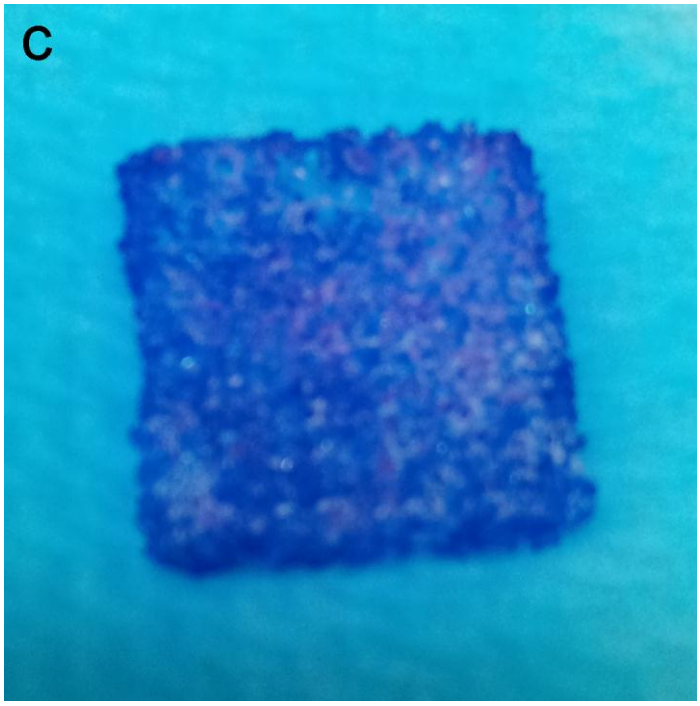

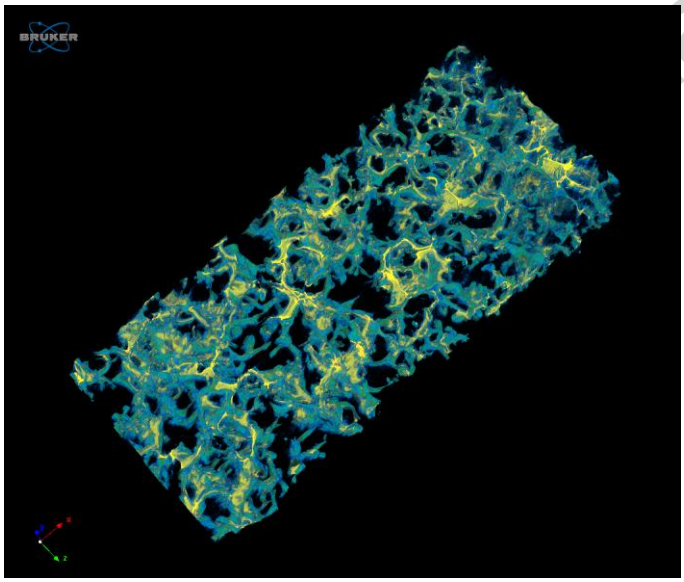

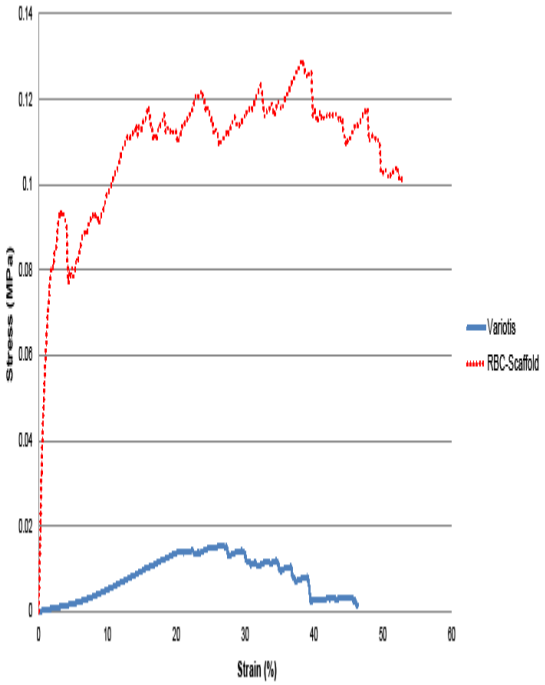

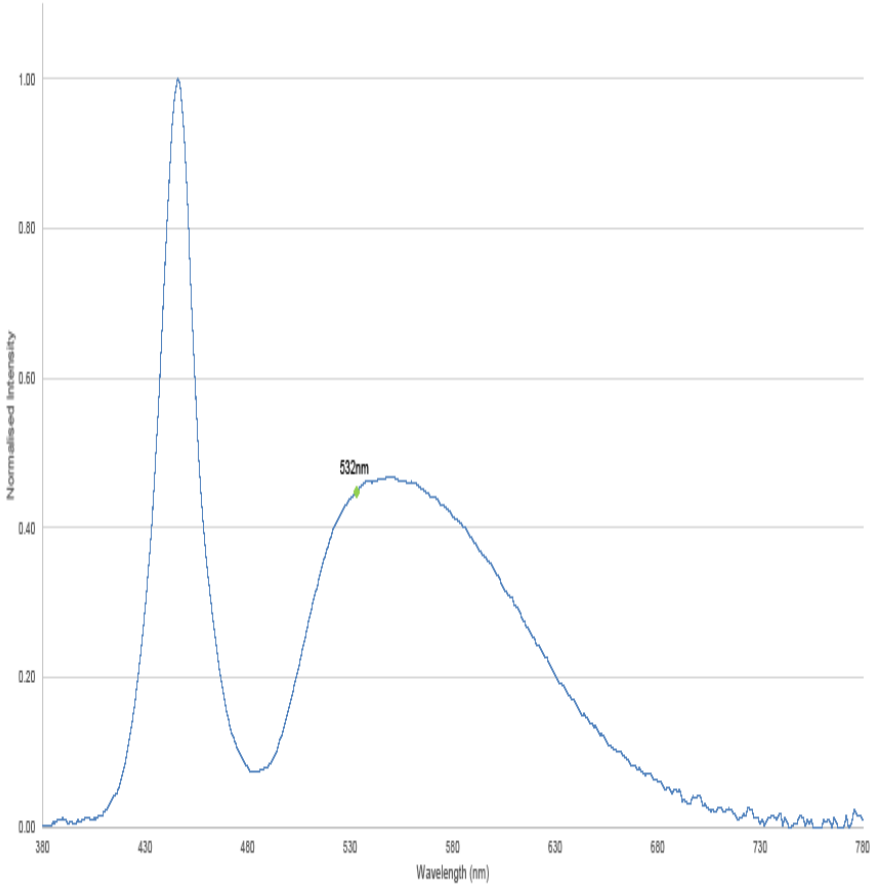

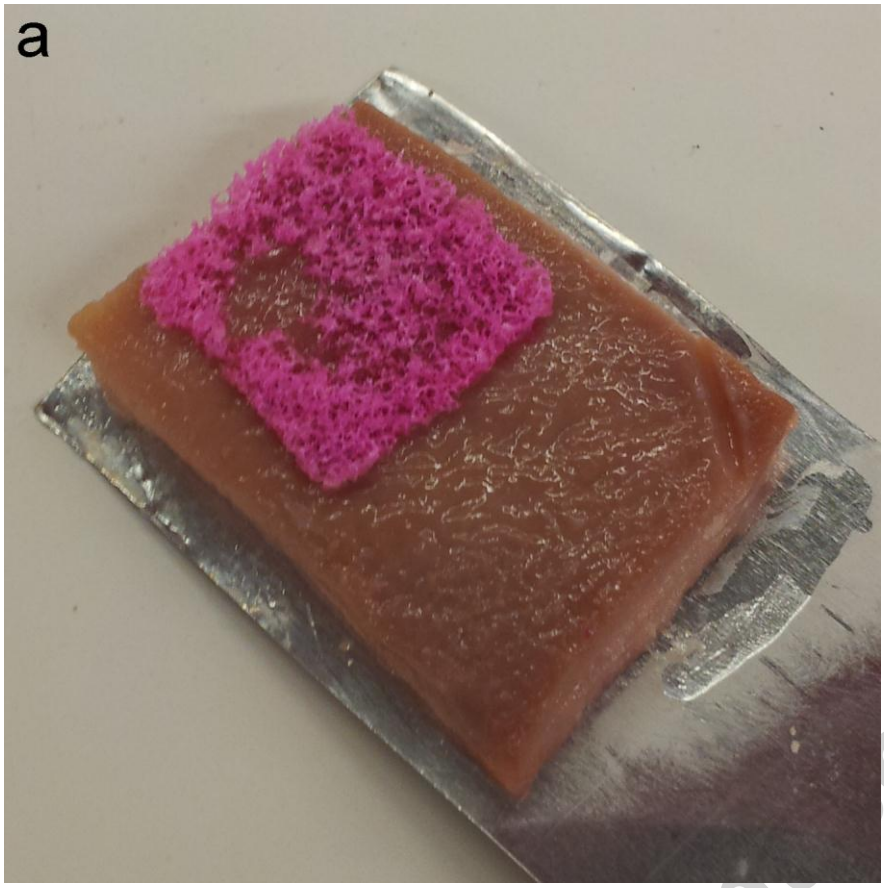
a

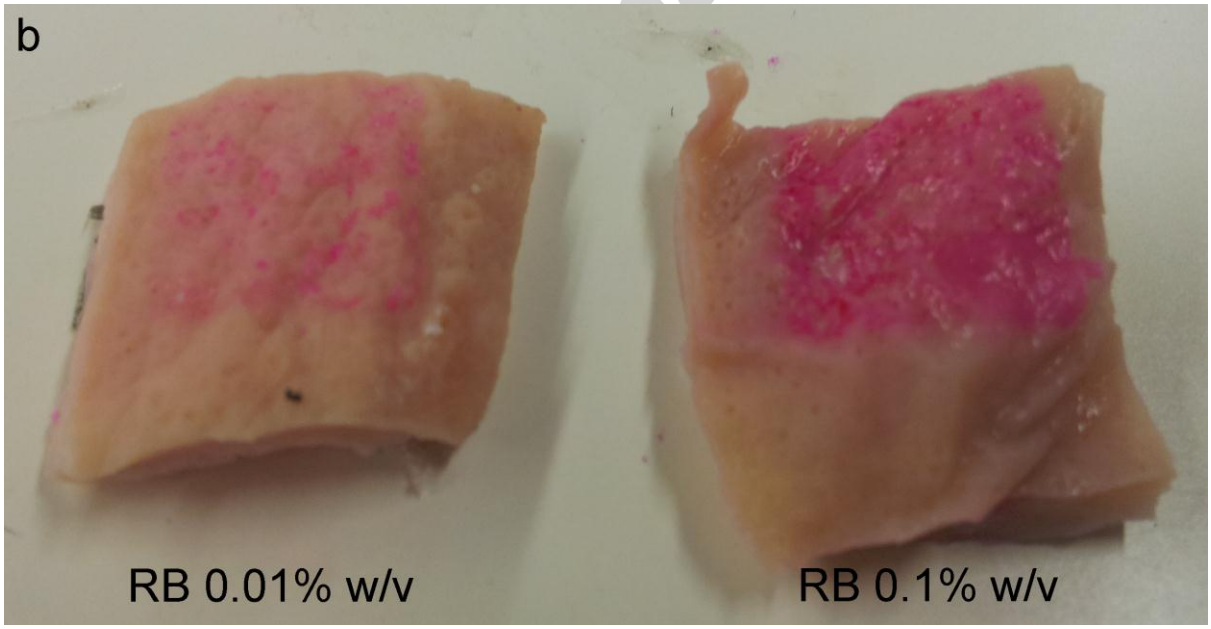
b
RB 0.01% w/v
RB 0.1% w/v

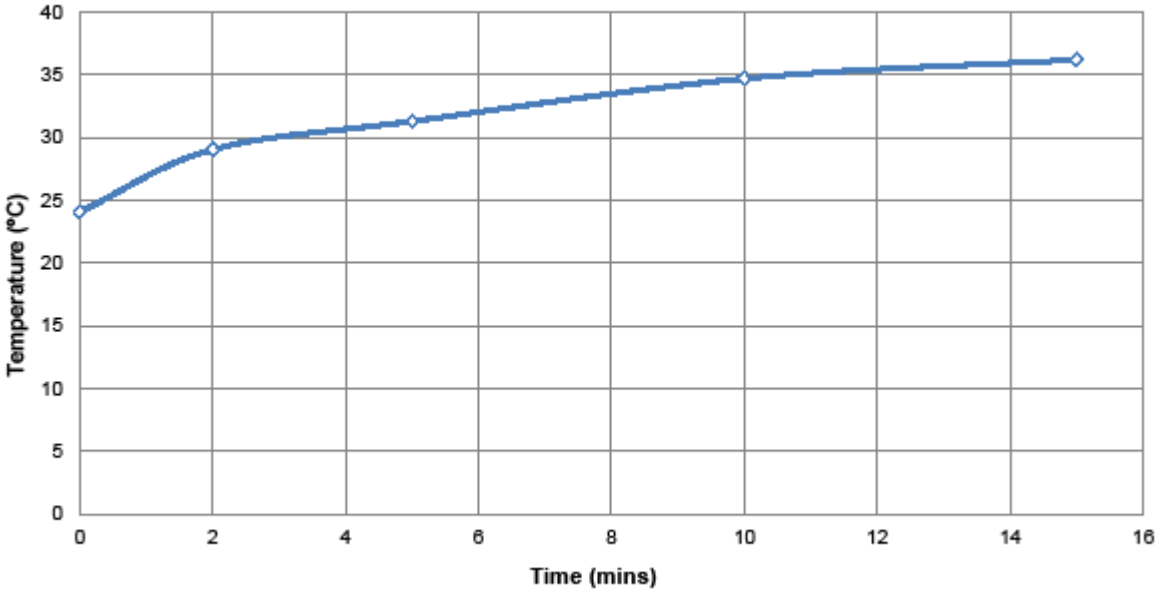
Temperature (°C)
Time (mins)
0
5
10
15
20
25
30
35
40
0
2
4
6
8
10
12
14
16

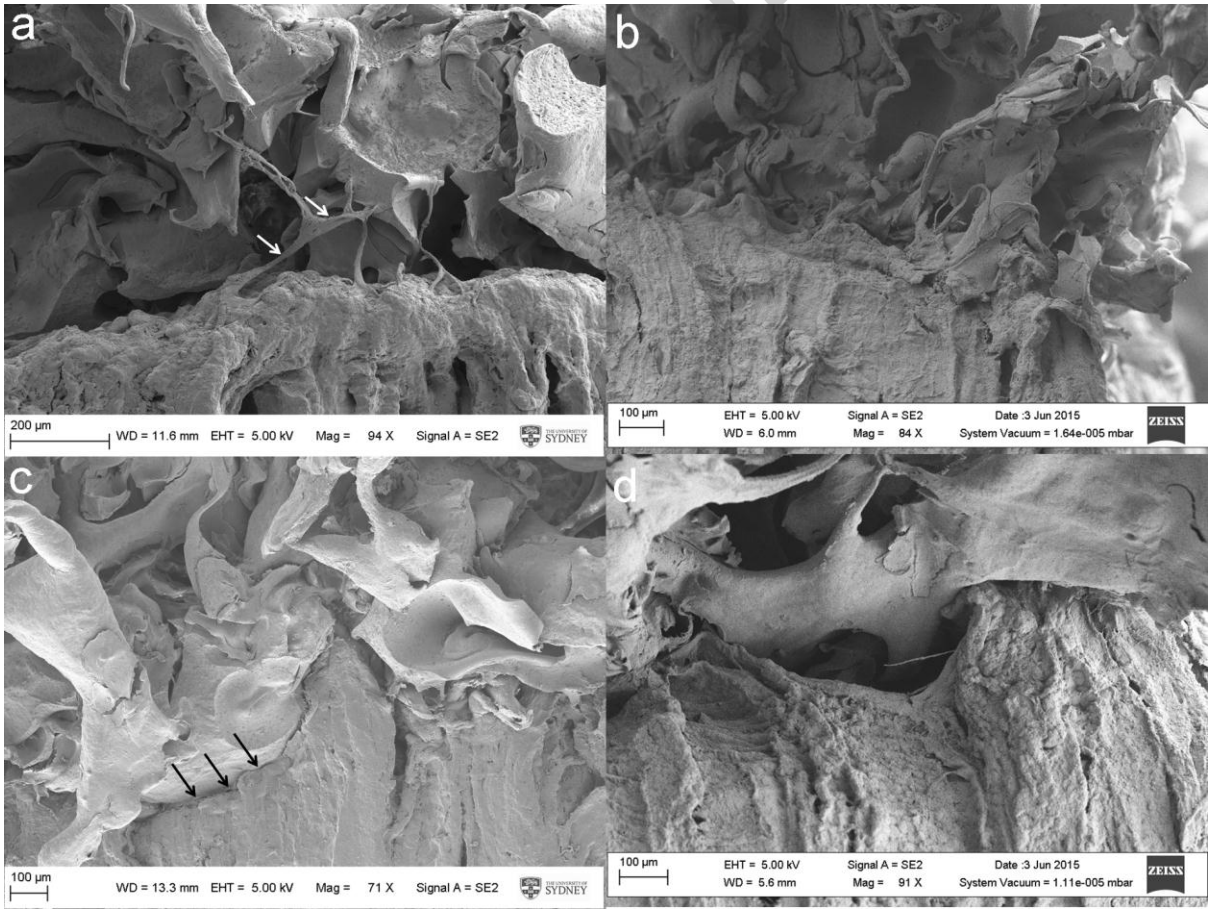
a
200 µm
WD = 11.6 mm EHT = 5.00 kV Mag = 94 X Signal A = SE2
b
100 µm
EHT = 5.00 kV Signal A = SE2 Date :3 Jun 2015
WD = 6.0 mm Mag = 84 X System Vacuum = 1.64e-005 mbar
c
100 µm
WD = 13.3 mm EHT = 5.00 kV Mag = 71 X Signal A = SE2
d
100 µm
EHT = 5.00 kV Signal A = SE2 Date :3 Jun 2015
WD = 5.6 mm Mag = 91 X System Vacuum = 1.11e-005 mbar

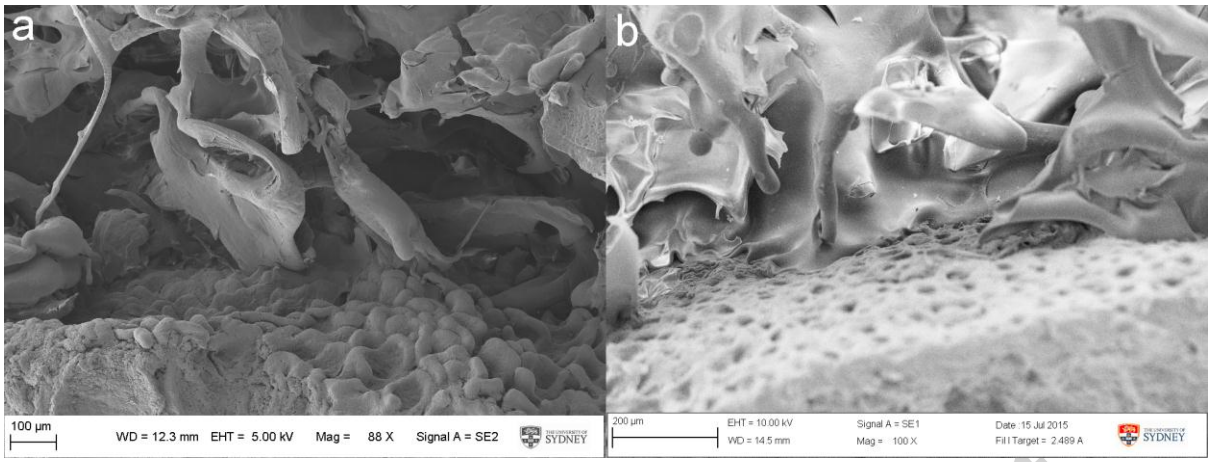

8.1 Highlights

- Light-activated Adhesive Scaffold successfully developed
- Achieved adhesive strength between soft tissue and scaffold of 8.61 ± 2.81 kPa
- Scaffold has properties conducive for tissue integration
- The potential for use in device attachment is high